PCCP

Comprehensive Study of Cold Protonated Tyramine : UV Photodissociation Experiments and ab initio Calculations

Journal:	*Physical Chemistry Chemical Physics*
Manuscript ID:	CP-ART-03-2015-001375.R1
Article Type:	Paper
Date Submitted by the Author:	17-Apr-2015
Complete List of Authors:	Broquier, Michel; CNRS UMR 8214 - Université Paris Sud, Institut des Sciences Moléculaires d'Orsay; LUMAT, CNRS FR 2764 - Université Paris Sud, Centre Laser de l'Université Paris Sud (CLUPS) Soorkia, Satchin; CNRS UMR 8214 - Université Paris Sud, Institut des Sciences Moléculaires d'Orsay Gregoire, Gilles; CNRS UMR 8214 - Universite Paris Sud, Institut des Sciences Moléculaires d'Orsay

Comprehensive study of cold protonated tyramine : UV photodissociation experiments and ab initio calculations

Michel Broquier,[1,2] Satchin Soorkia[1] and Gilles Grégoire[1*]

[1] *CNRS, Université Paris Sud, Institut des Sciences Moléculaires d'Orsay (ISMO) UMR 8214, 91405 Orsay Cedex, France*
[2] *Université Paris Sud, CLUPS (Centre Laser de l'Université Paris Sud) LUMAT FR 2764, 91405 Orsay Cedex, France*

*Corresponding author: gilles.gregoire@u-psud.fr

Abstract

We present a comprehensive experimental study of protonated tyramine ions in a cold 3D quadrupole ion trap coupled to a time-of-flight mass spectrometer. Multiple UV photodissociation techniques have been developed, including single and double resonance spectroscopy along with time-resolved excited state lifetime measurements through a picosecond pump-probe scheme. An original UV-UV hole burning method is presented which can be used without modification of the quadrupole ion trap. The electronic spectrum of the cold protonated tyramine exhibits well-defined vibronic transitions, allowing the firm assignment of its two low-lying energy conformations by comparison with CC2 *ab initio* excited state calculations.

1. Introduction

Photo reactivity, and in particular fragmentation, is a special class of molecular reaction that involves complex mechanisms, including charge transfer, electronic coupling, nuclear rearrangement, internal conversion and intersystem crossing processes. Studying the reactivity of ions in the gas phase indeed provides the ideal means to explore these fundamental aspects of the physical and chemical sciences, at the frontier of several research fields like astrophysics or biology. It requires the precise control of the initial state of the parent ions, the exact amount of energy imparted in the system and the knowledge of all the fragmentation pathways to get conclusive information on the molecular reactivity.

Research in the past fifteen years has shown considerable progresses in that way. While many efforts have been devoted to the study of neutral model systems, investigation of ionic species has just emerged in the very recent years, thanks to the combination of mass

spectrometry with laser spectroscopy. A major breakthrough has been achieved in the last decade in this domain with the advent of cold ion traps, which allow investigating ionic systems at low temperature, suitable to get precise spectroscopic data on well-defined molecular structures. The group of T. R. Rizzo in Lausanne has pioneered the study of IR/UV photodissociation spectroscopy on cold biomolecular ions[1] of larger and larger sizes.[2] In this experiment, a 22-pole linear ion trap, initially developed by Gerlish et al.,[3] mounted on a cold head of a cryostat, allows reaching vibrational temperature of 10 K. Very recently, the same group has shown that low vibrational temperature can be reached in a simplified octople ion trap.[4] Such experiments constitute the state-of-the-art for photofragmentation of cold biomolecular ions, which has stimulated other international research groups to develop such experiments using linear ion trap.[5] Wang *et al.*[6] have shown that low vibrational temperature could also be reached using a 3D quadrupole ion trap (QIT). The main advantages of such ion trap device rely on the rather ease to setup along with its interface with a time-of-flight mass spectrometer[7] providing the full photodissociation mass spectrum at once. Such 3D QIT device is now used by several research groups, for IR[8, 9] and UV[10, 11] photodissociation spectroscopy studies on cold molecular ions.

A new experimental apparatus comprising a cryogenic cold quadrupole ion trap (QIT) has been recently implemented at the laser facility of the University Paris Sud (CLUPS). It allows recording the electronic spectrum of gas phase ions through the detection of all the ionic photo fragments in a linear time-of-flight mass spectrometer. The cold temperature achieved in the QIT (about 10 K) along with the set of available tunable lasers offer great opportunities for the precise studies of gas phase reaction of molecular ions, depending on their conformations and with a control of the excess energy deposited in the system. Besides, we have set a picosecond pump-probe excitation scheme in order to record the conformer and mode selected excited state lifetime of protonated ions.[12] In a continuing effort to implement new UV spectroscopic techniques, following the recent works of Choi *et al.*[13] and Jouvet *et al.*,[14, 15] we present an original method to record the UV-UV hole burning spectra of molecular ions in a QIT.

We have recently reexamined the UV photo induced reaction of protonated phenylalanine and tyrosine, with an emphasis on their fragmentation branching ratio for the different conformers and as a function of the excess energy above the origin transition.[16] The photochemistry of these protonated aromatic amino acids is indeed very rich and complex. Several fragmentation pathways following UV photoexcitation are in competition, leading to different ionic fragments. Besides, the branching ratio between the fragmentation channel

evolves drastically with the excess energy imparted in the electronic ππ* excited state and can depend on the probed conformer. A general model has been presented recently which emphasizes the role of the low-lying optically "dark" $\pi\pi_{CO}$* and $\pi\sigma_{NH3}$* states and their possible coupling with the locally excited ππ* state.[16]

In this paper, we present a complete set of UV photodissociation techniques on a model system, protonated tyramine ions ($TyraH^+$). Such protonated aromatic amine molecule provides a simplified model system as compared to the natural occurring amino acid tyrosine. In $TyraH^+$, the only charge transfer state involved in the deactivation process corresponds to an electron transfer from the aromatic ring to the protonated ammonium group ($\pi\sigma_{NH3}$*) which should, in principle, ease the understanding of the photofragmentation process. Its spectroscopy has been recently reported by Feraud *et al.*[17] on a wide spectral range but with a moderate laser resolution (8 cm^{-1}), precluding a fine spectroscopic study. We have recorded the electronic absorption spectrum around the band origin with a higher spectral resolution and performed the UV-UV hole burning spectroscopy that allows the assignment of two conformers. Finally, we have investigated the excited state lifetimes of these conformers as a function of the excess energy imparted in the excited state. All these experimental results are compared to *ab initio* quantum chemistry calculations done at the couple cluster level CC2, including ground and excited state optimizations along with the frequency calculations and estimation of energy barriers for the proposed deactivation processes.

2. Experimental methods

The experimental setup, schematically presented in Fig. 1, is composed of an electrospray ionization source (ESI), a quadrupole ion trap, and a linear time-of-flight mass spectrometer (TOF-MS). Protonated tyramine ions are produced in the ESI source[18] from a solution of water/methanol (1:1 in volume) at a concentration of ~100 μM. At the exit of the capillary, ions are stored in an octopole trap for 100 ms by adjusting the voltage of the exit cap of the octopole a few volt higher (10 V) than the bias of the octopole (3 V). They are extracted by applying a pulsed negative pulse (-20 V, 5 μs width) on this exit cap and are further accelerated at -200 V by applying a second pulsed voltage (6 μs width) on a first Gauss tube of 5 cm long located just after the octopole exit electrode. When the ions are inside the Gauss tube, the voltage is switched back to ground, so they exit the tube in a field-free region. This time sequence produces ion packets with a temporal width of less than 1 μs and allows the mass selection of the ions of interest (at a given m/z) according to their time-

of-flight (TOF) to the QIT (Jordan ToF Inc.). Mass selection is done with a pulsed mass gate located 40 cm downstream. The mass gate is held at an electric field of 200 V/cm and switched to ground during 500 ns at a given delay in order to let go through the ion of interest. Several electrostatic lenses are used to drive the ions from the ESI to the QIT, biased at 220 V to match the kinetic energy of the incoming ions and prevent collision induced dissociation during the loading. The QIT is mounted on a cold head (CH-204S, Sumitomo) of a compressed helium cryostat, maintained at T ~ 10 K. The ions are trapped and thermalized through collisions with helium buffer gas, which is injected by a pulsed valve 1 – 2 ms before the ions enter the trap. The photodissociation lasers are triggered after a minimum delay of 30 ms to ensure an optimal cooling of the parent molecules and the overall trapping time is fixed to 80 ms. Parent and fragment ions are then extracted from the trap by applying a negative pulsed voltage on the exit cap of the QIT (-350 V) and accelerated by a second pulsed voltage (-1350 V, few μs) on a Gauss tube of 30 cm long located 2 cm downstream to the field free region of the linear TOF mass spectrometer (mass resolution m/Δm of 1000 at m/z 200) and finally detected on a microchannel plate detector (Z-Gap MCP, Jordan ToF Inc). The electronic spectra are obtained by scanning the laser frequency and recording the signal of each fragment ion, normalized by the parent ion signal and the intensity of the laser.

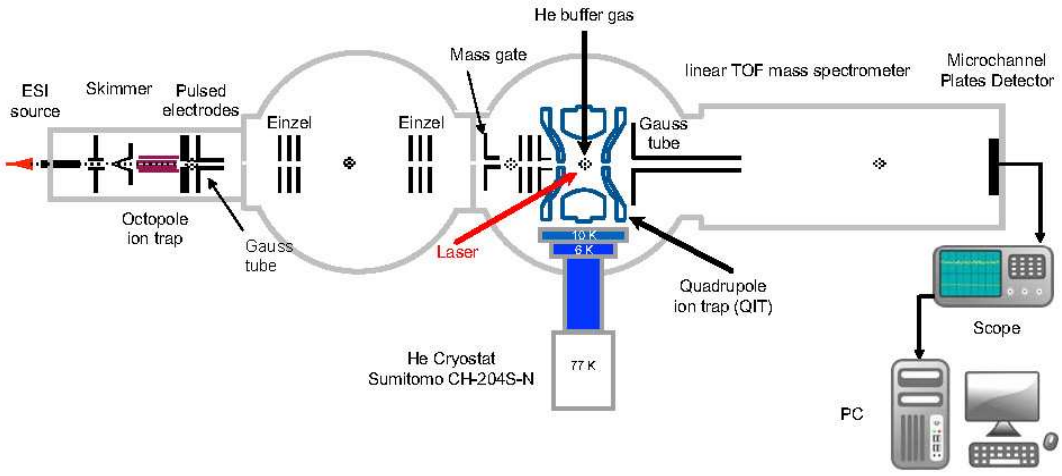

Fig. 1 Experimental setup comprising the ESI source, the cold quadrupole ion trap (QIT) and the linear time-of-flight mass spectrometer.

A set of UV photodissociation lasers has been used in this study. The electronic spectra of protonated tyramine (UV photodissociation and UV-UV hole burning) have been recorded with the two dye lasers (Quantel TDL 90), 0.2 cm^{-1} spectral resolution in the 285-280 nm region. The laser beams are collimated (2mm^2) into the QIT with an energy from 10

to 100 μJ/pulse. The electronic spectra (1 colour and hole-burning) are recorded with 32 laser shots per wavelength step. For the picosecond pump-probe experiments, the third harmonic (355 nm) output of a mode-locked picosecond Nd:YAG laser (EKSPLA-SL300 LT-02300), which operates at 10 Hz, pumps an optical parametric amplifier (OPA) (EKSPLA-PG411) to obtain tunable visible/UV light. The spectral resolution of the picosecond laser is about 10 cm^{-1}, and the temporal resolution in the order of 15 ps (cross correlation). Due to the lower laser intensity and spectral resolution of the picosecond laser, the pump and probe beams are focused in the QIT by 1m lenses to increase the photofragmentation yield. The laser pulses are delayed by a motorized optical delay line scanned in 6.6 ps step, and the transients are averages of 5 scans with 32 laser shots per scan step.

In any hole-burning spectroscopy through an ionization or fluorescence scheme, a first laser (burn) is scanned over the spectral domain while a second laser (probe), delayed in time, is tuned on a selected transition of the electronic spectrum, leading to a constant ion signal monitoring the population of a given conformation. Any dip in the constant signal is then assigned to a depleted population induced by the burn laser of the probed conformation. In a hole-burning spectrum through a UV phototodissociation scheme, both burn and probe lasers will produce the same photo fragments. Therefore, one needs to differentiate in the mass spectrum the fragment ions of a given m/z issued from the burn and probe lasers. The first UV-UV hole burning spectrum in a QIT trap has been reported by Choi *et al.*.[13] They observed that the light photo fragments can directly escape from the QIT when the probe laser is triggered at specific time delays with the same period than the trapping RF (900 kHz). In that way, the fragment ions issued from the burn and probe laser can be distinguished through their time-of-flights (TOF). Recently, Kang *et al.*[14] have proposed an elegant UV-UV hole burning method in a QIT. It relies on the ejection of the fragment ions produced by the burn laser by applying a RF voltage (tickle) whose frequency is adjusted resonantly to the mass of interest. The auxiliary RF destabilizes the trajectory of the fragment ion of a given mass in the QIT until their loss. With the low peak-to-peak voltage used (less than 1V), it takes about 10 ms to resonantly remove the fragment of interest. This rather long time sequence allows triggering the probe laser a few μs before the ejection of the ions from the trap, and the photofragmentation mass spectrum induced by the probe laser can thus be recorded as in normal conditions.

We present an alternative method that allows discriminating the fragment ions of a given m/z produced either by the burn or probe lasers through their distinct time-of-flights. It requires to accurately adjust the delay of the probe laser compared to the extraction of the ions

from the QIT while the burn laser can be fired anytime before the ion extraction pulse. Note that the trigger signal of the extraction voltage is also the one of the TOF mass spectrometer. To get a different TOF for the fragment ions produced by the probe laser, it is triggered within the rise time of the extraction pulse. This causes the fragment ions to be less accelerated than those formed by the burn laser. In our setup, the pulse voltage is set at 350 V with a rising time of 80 ns (Jordan TOF Inc.). The trigger time of the probe laser is accurately tuned by 10 ns step within this rising time with a home-made digital pulse generator. Thus, the photo fragments issued from the two excitation lasers are not extracted with the same potential and arrived at the MCP detector with different time-of-flights. As seen in Fig. 2, the optimal time separation for the m/z 121 fragment ion of TyraH+ is in the order of 50 ns for a 19 μs TOF, which is twice larger than the mass resolution of our linear TOF-MS. In principle, this scheme can be applied as long as the difference in TOF for the fragment ion is larger than the mass resolution of our linear TOF mass spectrometer, which puts a mass limit to about m/z 500 fragment ion. A simple way to increase the mass limit would be to use a reflectron TOF mass spectrometer. Within this scheme, the two lasers are fired at 10 Hz, and allows recording at the same time both the electronic spectrum of TyraH+ (first peak marked with a star) and the hole-burning spectrum as a dip in the constant signal (second peak marked with a cross) as soon as the same conformer is burned by the first laser.

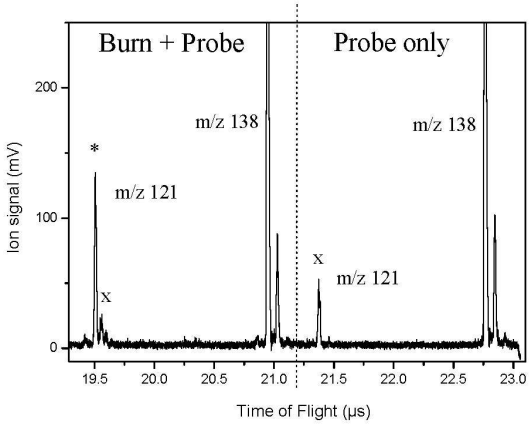

Fig. 2 Time-of-flight of $TyraH^+$ (m/z 138) following UV excitation recorded with the double trigger signal sent to the scope. The photodissociation signals produced by the burn+probe lasers and the probe laser only are recorded at the same time. On the left part of the TOF spectrum (burn+probe), the m/z 121 ionic fragment is produced either by the burn laser (star) or the probe laser (cross).

To improve the hole-burning signal-to-noise ratio, we run the burn laser at 5 Hz, while keeping the probe at 10 Hz and perform the experiment using the modified active baseline subtraction methods (ABS).[19, 20] It requires to record independently the signals produced by

the burn+probe lasers (5 Hz) and by the probe laser only (10 Hz) and to subtract them. In our case, a homemade digital pulse generator sends a double trigger signal to the scope recording the TOF. The two TOFs reported in Fig. 2 correspond to the burn+probe (5 Hz) and probe only (10 Hz) photodissociation mass spectra. The delay between these two trigger signals (1.8 μs in Fig. 1) is adjusted to split the two TOFs to ensure no overlap of the mass peaks. In this configuration, the burn laser can be either scanned across the excitation spectrum of the molecule with a fixed probe laser or tuned on a vibronic transition of the molecule while the probe laser is scanned to record the electronic spectrum. A better signal to noise ratio was found with this latter configuration. In that case, a hole-burning spectrum is obtained by subtracting the fragment ion signal of the burm+probe trace (cross peak) with the probe only trace (cross peak). As it can be seen on Fig. 2, a 30-50 % depleted signal is reached, and the full HB spectrum can be obtained within one single probe laser scan. It is noteworthy that this method allows fixing a short time delay between the burn and probe lasers, around few hundreds of nanosecond, while the method reported by Kang *et al.*[14] requires a delay of 10 ms or more to remove the fragments produced by the burn laser. This short delay between the laser pulses is not a mandatory condition to perform the UV-UV hole burning but ensure that the ion cloud has practically not moved and reduce the probability of repopulation of the burned conformer. Finally, it should be stressed that this UV hole-burning technique requires that the fragment ions are promptly produced following the laser excitation. If the fragmentation time is larger than the μs time scale, then the tickle method[14] must be used.

3. Theoretical modelling

Ab initio calculations have been performed with the TURBOMOLE program package (v6.2)[21] making use of the resolution-of-the-identity (RI) approximation for the evaluation of the electron-repulsion integrals.[22] The equilibrium geometries of protonated tyramine in the ground electronic (S_0) and excited states ($S_{n=1,2}$) have been determined at the CC2 level. In construction of the reaction path in the excited state for the proton transfer reaction from NH_3^+ to the cycle and the ammonia loss, the coordinate-driven minimum-energy-path (MEP) approach was utilized, *i.e.* for a given N-H or C-N distances, all remaining intramolecular coordinates were optimized in the S_1 state. Calculations were performed with the correlation-consistent polarized valence double-zeta aug-cc-pVDZ basis set augmented with diffuse functions.[23] The vibrational modes of the ground and the first excited states have been

calculated at the same level and the Franck-Condon analysis has been performed using PGOPHER software.[24]

4. Results

4.1. Electronic spectroscopy

The UV photodissociation mass spectrum of $TyraH^+$ is reported in Fig. 3a along with the excitation spectra (Fig. 3b) recorded on two distinct fragments at m/z 121 and m/z 108. In the plotted difference mass spectrum (laser on – laser off), positive mass peaks are issued from the photodissociation of the parent molecule $TyraH^+$ at m/z 138 (negative peak). $TyraH^+$ mostly fragments through the loss of NH_3 (m/z 121), which is the main fragmentation channel observed under low energy collision conditions. At higher energy collision, this ion undergoes secondary fragmentation leading to an ion at m/z 93. There are two other low yield fragments at m/z 108 and m/z 109 that are specific to UV photoexcitation. These two ions are issued from the C_α-C_β bond cleavage. Ion at m/z 108 is formed following proton transfer from NH_3^+ to the cycle in the excited state as already observed in protonated Phenylethylamine[17] and the amino acid analogues Tyrosine and Phenylalanine.[16] The other fragment at m/z 109 corresponds to a di hydrogenated fragment as already observed after 266 nm excitation in the case of $TyraH^+$,[25] $TryptophanH^+$,[26] and $TryptamineH^+$.[27]

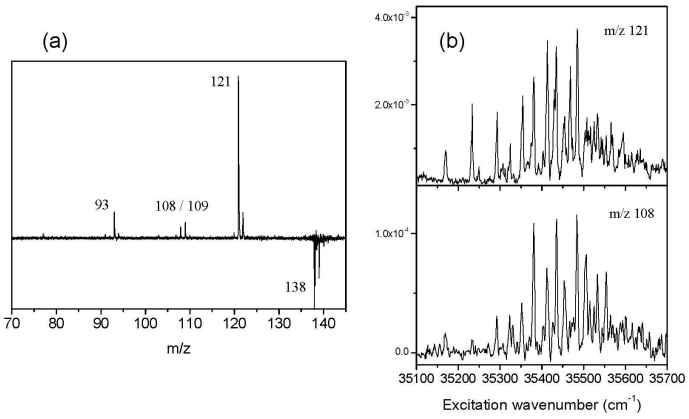

Fig. 3 (a) Difference mass spectrum (laser on – laser off) of $TyraH^+$ (m/z 138) at 35 480 cm^{-1}. The main fragment is m/z 121 (NH_3 loss), with its secondary fragment at m/z 93. The two ions at m/z 108 and m/z 109 are specific to UV excitation and issued from the C_α-C_β bond cleavage following proton transfer to the cycle. (b) Excitation spectrum of $TyraH^+$ recorded on m/z 121 (top) and m/z 108 (bottom). For m/z 108, some intense transitions seen on the other fragmentation channels are not or barely detected.

The electronic excitation spectrum of $TyraH^+$ has been recently reported on a large spectral range[17] but with a low spectral resolution, precluding a detailed spectroscopic study. Here, we report in Fig. 3b the excitation spectrum obtained at higher resolution in the vicinity of the band origin. The excitation spectrum is exactly the same for all fragments (m/z 121, 109, 93) except for ion at m/z 108 in which some intense transitions are not or barely seen. Such observation might be related to a conformer selectivity as already reported in the case of protonated tyrosine. However, the ion signal on this m/z 108 fragment is rather weak, which points out to a weak selectivity in the photodissociation mechanism. The excitation spectrum recorded on the m/z 121 ion has a first vibronic transition at 35 170 cm^{-1} and exhibits a vibrational progression of +63 cm^{-1}. Clearly, the Franck Condon activity is lower at the band origin than for the first vibronic bands. From 150-200 cm^{-1} above the band origin, the spectrum gets more dense and the last intense vibronic transition is detected at 35 484 cm^{-1}. In the excitation spectrum recorded at m/z 108, the first transitions from the band origin as well as at higher excitation energies are clearly absent or very weak. On this fragmentation channel, the first intense vibronic band is observed at 35 381 cm^{-1}. However, it is not clear whether or not this intense transition is indeed the band origin of another conformer or if there is a mode-selectivity in the photofragmentation pathway of $TyraH^+$. We have thus performed the UV-UV hole-burning spectra of $TyraH^+$ in order to reveal the contribution from the possible different conformations.

4.2 UV-UV Hole-Burning Spectroscopy

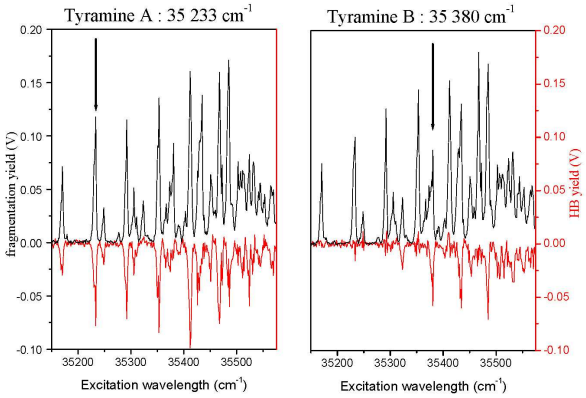

Fig. 4 UV-UV hole-burning spectra of $TyraH^+$ with the burn laser fixed at (A) 35 233 cm^{-1} and (B) 35 380 cm^{-1}.

The UV-UV hole burning (HB) spectra of $TyraH^+$ are reported in Fig. 4 by fixing the burn laser at wavelengths indicated by the arrows and recording the HB spectra at m/z 121 as explained in the experimental section. In the HB spectrum A (left panel), the burn laser is fixed at 35 233 cm^{-1}. The first transitions observed in the HB A spectrum correspond to the band origin at 35170 cm^{-1} along with the first two modes at +63 cm^{-1} and + 78 cm^{-1}, the former one having a greater intensity than the latter one. There is clearly a vibrational progression built on the mode at +63 cm^{-1} that extends up to 35 468 cm^{-1}. There are at least two bands that do not show up in the HB spectrum A in the vicinity of the band origin, i.e. at 35 323 cm^{-1} and 35 380 cm^{-1}. We have therefore recorded the HB spectrum B by fixing the burn laser on the intense transition at 35 380 cm^{-1} (right panel). All the transitions absent from the HB spectrum A now appear in the HB spectrum B, with a band origin of this second conformer at 35 323 cm^{-1} and a vibrational progression of + 57 cm^{-1} up to 35 484 cm^{-1}. It is noteworthy that the HB spectrum B resembles the one recorded at the m/z 108 fragment, with the same intense transitions. It thus seems that there is a weak conformer selectivity in $TyraH^+$. From the band origin up to 100 cm^{-1} of excess energy, conformer A almost exclusively fragments into m/z 121. The m/z 108/121 branching ratio then increases with the excess energy. For conformer B, both fragmentation channels are detected even at the band origin with the m/z 108/121 fragmentation branching ratio larger than for conf A. The hole-burning results confirm that only two conformers of $TyraH^+$ are populated at low temperature in the QIT. From the previous studies on protonated tyrosine,[28] they are thought to be the syn and anti conformers, corresponding to the orientation of the hydroxyl lone pair relative to the protonated ammonium group setting above the phenol plane (see 4.4.).

4.3. Picosecond pump-probe excitation scheme

We have also investigated the excited state lifetimes of the two conformers of $TyraH^+$ as a function of the excess energy. The excitation spectrum recorded on the m/z 121 fragment ion with the OPA ps laser from 35060 cm^{-1} to 35 650 cm^{-1} is reported in Fig. SI1 in supplementary information. It closely resembles the one previously reported in ref [17] with the 8 cm^{-1} resolution nanosecond OPA laser. The spectral resolution of the picosecond laser is in the order of 10 cm^{-1}, which is sufficient to resolve the main vibronic transitions observed in the higher resolution spectrum recorded with the nanosecond dye laser. This spectrum shares similarities with the excitation spectrum of protonated tyrosine,[12] in particular the intense transition about 805 cm^{-1} above the band origin, which is assigned to the excitation of mode 1 in the $\pi\pi^*$ state (see Fig. SI1). The vibronic progression observed from mode 1 at + 805 cm^{-1}

is the same as the one built from the band origin. So the vibronic transition in the higher energy range can also be assigned confidently. As already mentioned in the case of protonated tyrosine, this spectrum can be assigned to the excitation of the ππ* state up to 1500 cm^{-1} above the band origin. For clarity sake, all the transitions assigned to the conformer A are noted with a cross while those assigned to conformer B are noted with a star (see Supplementary Information). These marked bands have been used to follow the evolution of the excited state lifetimes of the two conformers of $TyraH^+$ as a function of the excess energy.

The principle of the measurement of the excited state lifetimes of protonated molecules through a pump/probe photodissociation scheme has been explained in our previous studies on protonated tryptamine[27] and tyrosine.[12] It relies on the change in the fragmentation branching ratio with the probe laser. We reported the transient recorded with the probe wavelength at 540 nm, and checked that the two-colour signal is independent of the probe wavelength (from 355 nm to 600 nm). The probe laser strongly affects the fragmentation branching ratio, with a decrease of the fragmentation yield of ions m/z 121 and m/z 93, and a concomitant increase of the fragmentation yield of m/z 108 ion. The intensity of m/z 109 ion is basically unchanged upon the excitation of $TyraH^+$ by the probe laser. This finding corroborates what has been already observed for this di hydrogenated aromatic fragment in the case of tryptamine[27] and tryptophan.[29] Besides, there is a new fragmentation channel which appears with the probe laser, *i. e.* the H-loss channel at m/z 137. This fragmentation channel is indeed observed in the case of $TyraH^+$ when excited within a one-colour scheme with an onset of 0.5 eV above the band origin.[17] In the two colour experiment, the total excess energy imparted in the system by the absorption of the pump and probe photons is well above this threshold. The nascent radical cation m/z 137 is thus produced with a large excess energy and can further fragment into its main secondary fragmentation channel at m/z 108.[30] Therefore, we can assume that the increase of the fragmentation yield observed at m/z 108 is related to the secondary fragmentation of the hot tyramine radical cation. This observation is consistent with the femtosecond pump-probe signals obtained on protonated tryptophan[31] and tryptamine.[27]

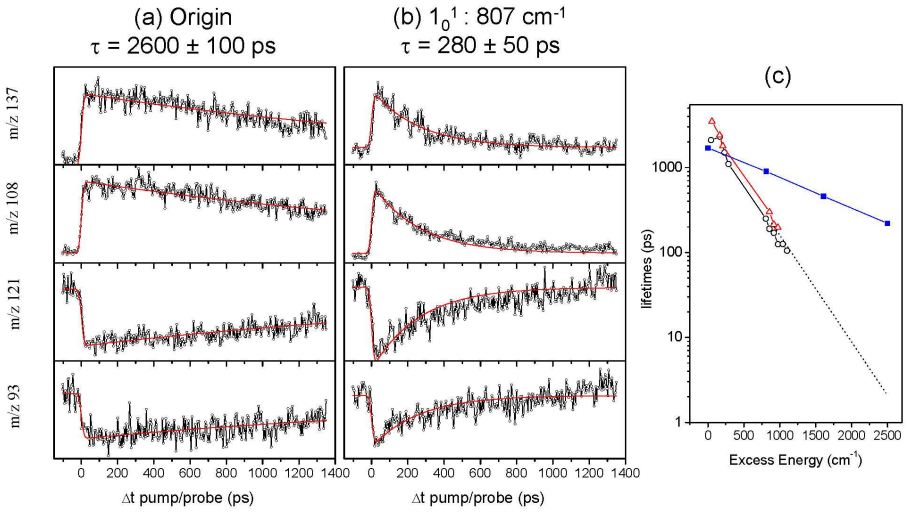

Fig. 5 (a) and (b) Excited state lifetime (picosecond) of $TyraH^+$ syn as the function of the excited vibrational mode in S_1 recorded on the different fragmentation channel m/z 137 and m/z 108 (issued from the H atom loss reaction) and m/z 121 and m/z 93 (issued from NH_3 loss). (c) Linear evolution (log y scale) of the excited state lifetime of $TyraH^+$ syn (black open circle) and anti (red open triangle) as a function of the excess energy in S_1. The same evolution for protonated tyrosine syn (blue filled square) conformer is reported for comparison.[12]

The time evolution of conformer A of $TyraH^+$ as a function of the delay between the pump and probe lasers are reported in Fig. 5 for two excitation wavelengths, corresponding to the excitation of the 0_0^0 and 1_0^1 bands. The signals are fitted with a single exponential decay function starting at zero delay time t_0, with a time constant τ accounting for the ππ* excited state lifetime, convoluted by a Gaussian function of width l_0 to account for the finite temporal profile of the laser beams (cross correlation of 15 ps), leading to the equation (1) :

$$S(t) = S_0 + \frac{S_1}{2}\left[1 + erf\left(\frac{t-t_0}{l_0}\right)\right]\exp-\left(\frac{t-t_0}{\tau}\right) \qquad (1)$$

For each excitation wavelength, the only adjustable parameters of the fit function are the excited state lifetime τ and the amplitudes of the pump signal only (S_0 background signal before time t_0) and two-colour pump/probe signals S_1 specific of each fragmentation channel. Note that in all cases, the sum over all the fragment ions of the S_1 amplitudes is null, ensuring that the probe laser does not enhance the overall fragmentation yield of $TyraH^+$ but solely changes the fragmentation branching ratio.

It is clear from the transients reported in Fig. 5 that the excited state lifetime decreases upon the excess energy in the excited state. We have reported in Fig. 5c the measured excited

state lifetimes for the two conformers of $TyraH^+$ that follows a linear evolution (on a log y scale) as a function of the excess energy above the origin band. Both conformers have, within the experimental uncertainty, the same excited state lifetimes. This evolution is qualitatively similar to the case of protonated tyrosine (filled blue square), although the decrease in the excited state lifetimes is much more rapid in this present case. While the excited state lifetime at the band origin for both molecules is in the order of 2-3 ns, it drops down to less than 300 ps for the 1_0^1 band (+800 cm^{-1}) of $TyraH^+$ while being 900 ps for protonated tyrosine. At +1100 cm^{-1} of excess energy, the excited state lifetime of $TyraH^+$ is reduced to 100 ± 20 ps.

5. Discussion

5.1 ππ* excited state calculations: conformer assignments

Table 1: Energy (cm^{-1}) of the ground and first electronic states of the two conformers of $TyraH^+$ obtained by geometry optimization and frequency calculations at the CC2/aug-cc-pVDZ level.

	S_0	$S_1 - S_0$ exp	$S_1 - S_0$ calc	$\Delta 0_0^0$ exp syn/anti	$\Delta 0_0^0$ calc syn/anti
$TyraH^+$ syn (A)	0	35 170	34 633	153	174
$TyraH^+$ anti (B)	25	35 323	34 807		

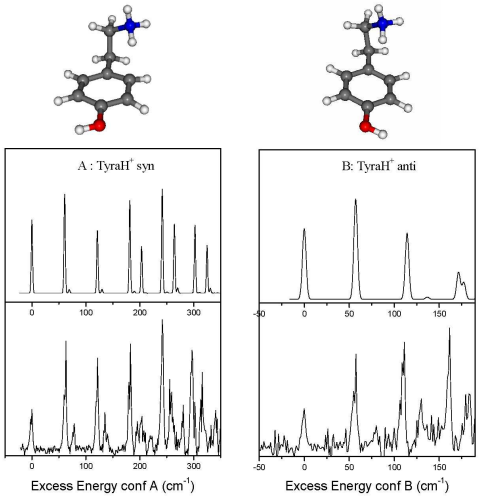

Fig. 6 Franck-Condon simulated spectra of (A) $TyraH^+$ syn and (B) $TyraH^+$ anti conformers obtained from frequency calculation at CC2/aug-cc-pVDZ level with the comparison with the two HB spectra found in Fig. 4. The origin of the two spectra is set to the band origin of the two conformers.

$TyraH^+$ can only adopt two low-lying energy conformations. They differ by the orientation of the hydroxyl lone pair relative to the ammonium group lying above the phenol plane, and are noted syn and anti, as reported in Fig. 6. In Table 1, we have reported the energetics of the ground and excited electronic states of $TyraH^+$ syn and anti conformers. We have calculated for the S_0 ground and S_1 excited states ($\pi\pi^*$) the optimized structures and their frequencies. Both conformers are basically iso energetic at this level of theory (CC2/aug-cc-pVDZ), with a difference of 25 cm^{-1} in favor of the syn conformer. The calculated adiabatic 0_0^0 transitions are corrected by the zero point energy difference between the ground and excited states. The agreement with the experimental values is remarkable, and only deviates by 1.5%. The calculated adiabatic 0_0^0 excitation energies of the two conformers differ by 174 cm^{-1}, the syn conformer having the reddest band origin, while the experimental difference is 153 cm^{-1}. The calculated Franck Condon spectra of both conformers are reported in Fig. 6 and compared to the two HB spectra A and B of Fig. 4. All the calculated spectra are convoluted by a Gaussian function of 3 cm^{-1}, and the origin transitions are scaled to the experimental values. For the two conformers, there are only a few low frequency modes that are active in this simulation, in agreement with the experimental spectra. These modes involve motions of the ammonium group along with out-of-plane bending of the aromatic CH group (see supporting information), as already reported in the case of protonated tyrosine.[16] In particular, the vibrational progression of the ν_1 mode calculated at 63 cm^{-1} and 59 cm^{-1}, for the syn and anti conformer respectively, accounts for the most intense transitions observed in the experimental spectra. The nice agreement between simulated and experimental electronic spectra allows assigning without ambiguity the syn conformer to the spectrum A and the anti structure to the spectrum B. It is noteworthy that, as reported by Stearn *et al.*[28] in the case of protonated tyrosine, the difference in the IR spectra of syn and anti conformers is too small to firmly assign the conformation of the molecules concerning the orientation of the hydroxyl group.

5.2 Deactivation processes

The main fragmentation channel following electronic excitation in $TyraH^+$ is the ammonia loss, leading to the ionic fragment at m/z 121. The other fragmentation channels, in particular those involving the C_α-C_β bond cleavage (m/z 108 and 109), are at least one order of magnitude less intense. This is quite at variance with protonated tyrosine for which the main ionic fragment formed around the band origin is m/z 108. In this latter case, we have

shown that a proton transfer reaction from the ammonium group toward the phenol ring has a low energy barrier of roughly 0.15 eV. We have thus calculated in the case of protonated tyramine the Minimum Energy Path (MEP) for the proton transfer to the ring. Interestingly, the calculated barrier (0.15 eV) is the same for both conformers and quite similar with the one calculated for protonated tyrosine. Therefore, it might have another efficient deactivation mechanism in competition with the proton transfer to the ring that accounts for the ammonia loss channel in $TyraH^+$.

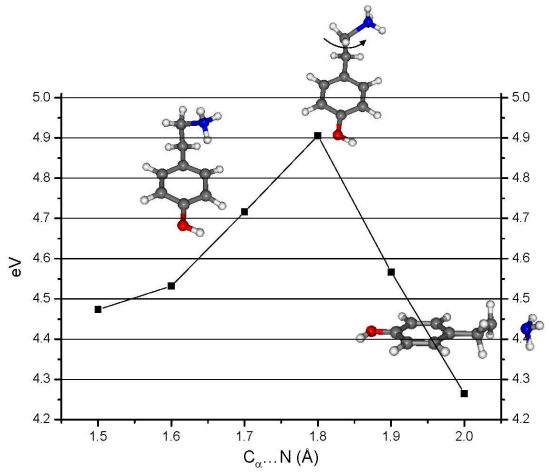

Fig. 7 Minimum Energy Path (MEP) for the loss of NH_3 in the S_1 excited state of $TyraH^+$ anti. The high energy barrier (0.5 eV) along with the large nuclear displacement at large C_α-N distances suggests that the C_α-N cleavage does not occur in the excited state.

We have calculated the MEP for the NH_3 loss directly from the ππ* state (Fig. 7). Such process has already been investigated in the case of protonated tryptamine, which exhibits a barrier of 0.25 eV,[32] higher than the one calculated for the H-loss. In this former case, the loss of ammonia has indeed been related to an internal conversion process following an aborted H-loss reaction in the excited state, and not to a direct fragmentation reaction in the excited state. In the case of $TyraH^+$, the calculated barrier in the excited state is even higher, around 0.5 eV. Besides, at C_α-N bond length of 1.8 Å, which corresponds to the top of the barrier, the ammonium group has rotated by $2\pi/3$ around the C_α-C_β bond backward the phenol ring. Starting from this optimized structure, the potential energy curve gets repulsive as the C_α-N bond length increases. During the course of the optimization, the m/z 121 ion has a planar structure with alkyl chain and the phenol ring in the same plane. The direct loss of ammonia from the ππ* state thus exhibits a quite large barrier with a significant nuclear rearrangement, and is not thought to be competitive as regard to the proton transfer to the ring.

An alternative mechanism should thus be invoked to account for the main fragmentation channel, and relies on the coupling of the locally excited ππ* state with higher electronic state. The second electronic state, S_2, has a πσ* character, where the active electron lies in a Rydberg-like orbital around the ammonium group. The $S_2 \leftarrow S_0$ vertical transition energy sets at 0.4 eV above the $S_1 \leftarrow S_0$ transition, independently of the two conformers. At the ππ* optimized geometry, the πσ*/ππ* gap is much larger, around 1 eV. We have performed the S_2 πσ* state optimization and found that the πσ* state crosses the S_1 state with a barrier of 0.3 ± 0.03 eV for the two conformers. The height of the barrier is significantly lower than the ππ*/ππ*$_{CO}$ barriers found in the cases of protonated tyrosine and phenylalanine, in the order of 0.4/0.6 eV.[16] In these protonated amino acids, the charge transfer state to the carbonyl has a lower energy barrier than the πσ*. In these latter cases, the competition between the C_α-C_β bond cleavage following proton transfer to the cycle detected at the band origin and the opening of the other fragmentation channels at higher excitation energies has been rationalized by the different height of the barriers for these two mechanisms. Besides, the proton transfer to the cycle involved large nuclear displacements, in particular ring puckering, which are thought to be dynamically in restraints as compared to the electron transfer processes. So in TyraH$^+$, due to the low ππ*/πσ* energy barrier, the main deactivation mechanism should involve the electronic coupling between the ππ* and the πσ* states.

As already mentioned in previous studies,[33] such electron transfer from the ring to the ammonium group leads to the formation of a hypervalent, unstable C_α-NH_3 group. This radical species can dissociate through either the H loss or the NH_3 loss. As explained previously, the direct loss of ammonia in the excited state is not thought to be a competitive process. However, experimentally, the H loss channel is observed in TyraH$^+$ about 0.5 eV above the origin transition. This has been previously rationalized by a simple energetic model.[34] The dissociative πσ* state crosses the ground state at larger N-H distance, but the H loss is hindered at the band origin due to its higher dissociation limit as compared to the excitation energy, so the system evolves to the ground state after internal conversion. In TyraH$^+$, the main fragmentation channel observed in collision induced dissociation is the NH_3 loss, which might thus explain the observed fragmentation pattern following electronic excitation. The CC2 calculations give a qualitative picture of the deactivation mechanisms occurring in protonated tyramine, in particular the predominance of the charge transfer process to the ammonium leading to the ammonia loss against the proton transfer to the

aromatic ring leading to the m/z 108 ionic fragment. However, the weak conformer selectivity observed in conformer syn, *i. e.* the opening of the m/z 108 fragmentation channel about 100 cm^{-1} above the band origin, is certainly too subtle to be treated by the CC2 calculations.

Finally, it is noteworthy that the excited state lifetime in $TyraH^+$ decreases more rapidly with the excess energy than in the case of protonated tyrosine. The lower energy barrier to the $\pi\sigma^*$ charge transfer state in $TyraH^+$ than in protonated tyrosine somehow confirms this experimental trend. However, such dynamical process can not be treated by static calculations and will deserve state-of-the-art excited state molecular dynamics simulations.[35, 36] Besides, the determination of the electronic coupling between the $\pi\pi^*$ and $\pi\sigma^*$ states requires multiconfiguration *ab initio* calculations that are out of the scope of this study.[37] Our experimental result nevertheless suggests that the strength of the $\pi\pi^*/\pi\sigma^*$ coupling gets larger with a small excess energy in $TyraH^+$ than the $\pi\pi^*/\pi\pi^*_{CO}$ coupling in the protonated aromatic amino acids. These benchmark experimental results are challenging for theoretical predictions.

6. Conclusions

We have developed a versatile experimental setup comprising a cold quadrupole ion trap with a time-of-flight mass spectrometer for the electronic spectroscopic studies of cold biomolecular ions. Single and double resonance spectroscopy techniques are presented, including UV-UV hole burning and time-resolved pump-probe experiments. This set of spectroscopic methods allows assigning the molecular structure and investigating the fragmentation processes induced in the excited states of protonated tyramine ions by comparison with CC2 calculations. While this theoretical method gives some hints for the general understanding of the photo reactivity in these protonated biomolecules, these benchmark experimental results provide stringent challenges for state-of-the-art configuration interaction (CI) and multiconfigurational methods needed to account for the fine coupling between the electronic states.

Electronic Supplementary Information (ESI)

(1): Electronic spectrum of $TyraH^+$ recorded with the picosecond laser (10 cm^{-1} spectral resolution) over a wide spectral range. (2): details of the simulated Franck-Condon spectrum of $TyraH^+$ syn conformer.

Acknowledgments

This work has been supported by the Université Paris–Sud 11, by the ANR research Grant (ANR2010BLANC040501), the RTRA ‘‘Triangle de la Physique’’ COMOVA and COMOVA II. We thank C. Charrière from the electronic staff of the ISMO laboratory. We acknowledge the uses of the computing facility clusters GMPCS of the LUMAT federation (FR LUMAT 2764) and MAGI of the University Paris 13.

Notes and References

1 O. V. Boyarkin, S. R. Mercier, A. Kamariotis and T. R. Rizzo, *J. Am. Chem. Soc.*, 2006, **128**, 2816-2817.
2 T. R. Rizzo, J. A. Stearns and O. V. Boyarkin, *Int. Rev. Phys. Chem.*, 2009, **28**, 481-515.
3 D. Gerlich, *Advances in Chemical Physics*, 1992, **82**, 1-176.
4 O. V. Boyarkin and V. Kopysov, *Rev. Sci. Instrum.*, 2014, **85**.
5 J. G. Redwine, Z. A. Davis, N. L. Burke, R. A. Oglesbee, S. A. McLuckey and T. S. Zwier, *Int. J. Mass Spectrom.*, 2013, **348**, 9-14.
6 X. B. Wang and L. S. Wang, *Rev. Sci. Instrum.*, 2008, **79**, 073108.
7 S. M. Michael, M. Chien and D. M. Lubman, *Rev. Sci. Instrum.*, 1992, **63**, 4277-4284.
8 C. M. Leavitt, A. B. Wolk, J. A. Fournier, M. Z. Kamrath, E. Garand, M. J. Van Stipdonk and M. A. Johnson, *J. Phys. Chem. Lett.*, 2012, **3**, 1099-1105.
9 A. B. Wolk, C. M. Leavitt, E. Garand and M. A. Johnson, *Accounts of Chemical Research*, 2014, **47**, 202-210.
10 C. M. Choi, D. H. Choi, N. J. Kim and J. Heo, *Int. J. Mass Spectrom.*, 2012, **314**, 18-21.
11 I. Alata, J. Bert, M. Broquier, C. Dedonder, G. Feraud, G. Gregoire, S. Soorkia, E. Marceca and C. Jouvet, *J. Phys. Chem. A*, 2013, **117**, 4420-4427.
12 S. Soorkia, M. Broquier and G. Gregoire, *J. Phys. Chem. Lett.*, 2014, **5**, 4349-4355.
13 C. M. Choi, D. H. Choi, J. Heo, N. J. Kim and S. K. Kim, *Angew. Chem. Int. Ed.*, 2012, **51**, 7297-7300.
14 H. Kang, G. Feraud, C. Dedonder-Lardeux and C. Jouvet, *J. Phys. Chem. Lett.*, 2014, **5**, 2760-2764.
15 G. Feraud, C. Dedonder, C. Jouvet, Y. Inokuchi, T. Haino, R. Sekiya and T. Ebata, *J. Phys. Chem. Lett.*, 2014, **5**, 1236-1240.
16 G. Feraud, M. Broquier, C. Dedonder-Lardeux, C. Jouvet, G. Gregoire and S. Soorkia, *J. Phys. Chem. A*, 2015, DOI: 10.1021/jp5065837.
17 G. Feraud, M. Broquier, C. Dedonder, G. Gregoire, S. Soorkia and C. Jouvet, *Phys. Chem. Chem. Phys.*, 2014, **16**, 5250-5259.
18 L. H. Andersen, A. Lapierre, S. B. Nielsen, I. B. Nielsen, S. U. Pedersen, U. V. Pedersen and S. Tomita, *Euro. Phys. J. D*, 2002, **20**, 597-600.
19 T. S. Zwier, *Annu. Rev. Phys. Chem.*, 1996, **47**, 205-241.
20 A. Sen, V. Lepere, K. Le Barbu-Debus and A. Zehnacker, *ChemPhysChem*, 2013, **14**, 3559-3568.
21 R. Ahlrichs, M. Bar, M. Haser, H. Horn and C. Kolmel, *Chem. Phys. Lett.*, 1989, **162**, 165-169.
22 F. Weigend and M. Haser, *Theo. Chem. Acc.*, 1997, **97**, 331-340.

23 T. H. Dunning, *J. Chem. Phys.*, 1989, **90**, 1007-1023.
24 C. M. Western, PGOPHER, a Program for Simulating Rotational Structure, University of Bristol, Bristol, 2010.
25 B. Lucas, M. Barat, J. A. Fayeton, M. Perot, C. Jouvet, G. Gregoire and S. B. Nielsen, *J. Chem. Phys.*, 2008, **128**, 164302.
26 V. Lepere, B. Lucas, M. Barat, J. A. Fayeton, Y. J. Picard, C. Jouvet, P. Carcabal, I. Nielsen, C. Dedonder-Lardeux, G. Gregoire and A. Fujii, *Phys. Chem. Chem. Phys.*, 2007, **9**, 5330-5334.
27 H. Kang, C. Jouvet, C. Dedonder-Lardeux, S. Martrenchard, C. Charriere, G. Gregoire, C. Desfrancois, J. P. Schermann, M. Barat and J. A. Fayeton, *J. Chem. Phys.*, 2005, **122**, 084307.
28 J. A. Stearns, S. Mercier, C. Seaiby, M. Guidi, O. V. Boyarkin and T. R. Rizzo, *J. Am. Chem. Soc.*, 2007, **129**, 11814-11820.
29 G. Gregoire, B. Lucas, M. Barat, J. A. Fayeton, C. Dedonder-Lardeux and C. Jouvet, *Euro. Phys. J. D*, 2009, **51**, 109-116.
30 H. J. Guo, L. L. Ye, L. Y. Jia, L. D. Zhang and F. Qi, *Chin. J. Chem. Phys.*, 2012, **25**, 11-18.
31 H. Kang, C. Dedonder-Lardeux, C. Jouvet, G. Gregoire, C. Desfrancois, J. P. Schermann, M. Barat and J. A. Fayeton, *J. Phys. Chem. A*, 2005, **109**, 2417-2420.
32 G. Gregoire, C. Jouvet, C. Dedonder and A. L. Sobolewski, *Chem. Phys.*, 2006, **324**, 398-404.
33 G. Gregoire, C. Jouvet, C. Dedonder and A. L. Sobolewski, *J. Am. Chem. Soc.*, 2007, **129**, 6223-6231.
34 H. Kang, C. Jouvet, C. Dedonder-Lardeux, S. Martrenchard, G. Gregoire, C. Desfrancois, J. P. Schermann, M. Barat and J. A. Fayeton, *Phys. Chem. Chem. Phys.*, 2005, **7**, 394-398.
35 G. Tomasello, M. Wohlgemuth, J. Petersen and R. Mitric, *J. Phys. Chem. B*, 2012, **116**, 8762-8770.
36 M. Malis, Y. Loquais, E. Gloaguen, H. S. Biswal, F. Piuzzi, B. Tardivel, V. Brenner, M. Broquier, C. Jouvet, M. Mons, N. Doslic and I. Ljubic, *J. Am. Chem. Soc.*, 2012, **134**, 20340-20351.
37 L. Gonzalez, D. Escudero and L. Serrano-Andres, *ChemPhysChem*, 2012, **13**, 28-51.

Table of Content Graphic:
Excited state properties of cold protonated ions are revealed from a combination of laser spectroscopy and ab initio calculations.